Open Ceramics 10 (2022) 100268

Contents lists available at ScienceDirect

Open Ceramics

journal homepage: www.sciencedirect.com/journal/open-ceramics

Sintering of Li-garnets: Impact of Al-incorporation and powder-bed composition on microstructure and ionic conductivity

Sandra Lobe [a,*], Alexander Bauer [a], Doris Sebold [a], Nadine Wettengl [b], Dina Fattakhova-Rohlfing [a,c,d], Sven Uhlenbruck [a,c]

[a] *Forschungszentrum Jülich GmbH, Institute of Energy and Climate Research (IEK-1), Materials Synthesis and Processing, 52425, Jülich, Germany*
[b] *Forschungszentrum Jülich GmbH, Central Institute for Engineering, Electronics and Analytics (ZEA-3), Analytics, 52425, Jülich, Germany*
[c] *Helmholtz-Institute Münster, Ionics in Energy Storage (IEK-12), 52425, Jülich, Germany*
[d] *Faculty of Engineering and Center for Nanointegration Duisburg-Essen (CENIDE), Universität Duisburg-Essen, Lotharstraße 1, 47057, Duisburg, Germany*

ARTICLE INFO

Keywords:
$Li_5La_3Ta_2O_{12}$
Garnet
Sintering
Powder bed

ABSTRACT

Garnet-structured Li-ion conductors are promising candidates as electrolytes for all-solid-state batteries. However, sintering of these materials is still a challenge, due to Li-loss accompanied by decomposition at elevated temperatures. In this study, $Li_5La_3Ta_2O_{12}$, a garnet material with reduced Li-content, was used as a model material to investigate the impact of the Li content in powder beds as well as the presence of Al either in the green bodies or in the powder beds on the properties of the resulting sintered materials. The resulting relative densities were increased by sintering in a Li-rich powder bed compared to a powder bed with identical stoichiometry. Furthermore, Al either in the source material or in the powder bed was shown to support densification, even if it is not incorporated in the structure. The highest ionic conductivity was 3.4 × 10^{-5} S cm^{-1} at 30 °C for $Li_5La_3Ta_2O_{12}$, which was sintered in a $Li_{6.54}Al_{0.02}La_3Zr_{1.6}Ta_{0.4}O_{12}$ powder bed.

1. Introduction

All-solid-state batteries gain much interest due to the increased safety and energy density compared to state-of-the-art commercialized Li-ion batteries. Especially garnet-structured ceramic Li-ion conductors are promising candidates for battery application due to their high inherent safety, moderate ionic conductivity, high chemical and electrochemical stability, and particularly their high stability in contact with Li metal. Among different garnet structures, cubic Zr-based Li-stuffed garnet $Li_7La_3Zr_2O_{12}$ (LLZ) attracts the most attention due its highest Li-ion conductivity of up to 1.8 × 10^{-3} S cm^{-1} [1–5], which makes it the most promising electrolyte for the development of ceramic-based solid-state batteries. Serious challenges with respect to the practical integration of LLZ into all-solid-state batteries lie in the compatibility with other materials, i.e., particularly the reaction with cathode active materials at the temperature required for the densification of mixed cathodes [6–8]. The ionic conductivity of other garnet compositions is generally one or two orders of magnitude lower. $Li_5La_3Ta_2O_{12}$ (LLTaO), which was in fact the first garnet Li-ion conductor described by Thangadurai et al., in 2005 [9], demonstrates conductivities of about 10^{-6} S cm^{-1} to 10^{-5} S cm^{-1} at RT [9–15]. However, while exhibiting lower conductivity, LLTaO shows a higher thermal stability in conjunction with cathode materials like the high-voltage spinel $LiCoMnO_4$ [16]. Furthermore, the deposition of thin layers can be carried out at lower temperatures (e.g., 400°C [16]), because the thermodynamically preferred formation of $La_2Zr_2O_7$ below 660°C [17–19] cannot occur.

Table 1 summarizes conductivities of various sintered LLTaO materials obtained via different synthesis routes. The ionic conductivities are two or more orders of magnitude lower than the highest values observed for LLZ. However, in only a few reports the relative density of the specimens was taken into account. Therefore, it is unclear whether the low conductivities were due to low sample density or other causes. A comparison of the ionic conductivities resulting from different sintering temperatures shows that lower sintering temperatures yielded lower conductivities. Mariappan et al. [11] reported a relative density of only 71% for LLTaO sintered at 850°C. Sintering temperatures of 1150°C and higher led to increased relative densities as well as higher Li-ion conductivities. When special processing methods, such as a self-consolidation strategy [15] or the use of sintering additives, such as $NaHCO_3$ and α-Al_2O_3 [10], were applied, ionic conductivities of up to

---

* Corresponding author.
E-mail address: s.lobe@fz-juelich.de (S. Lobe).

https://doi.org/10.1016/j.oceram.2022.100268
Received 23 December 2021; Received in revised form 15 April 2022; Accepted 9 May 2022
Available online 13 May 2022

3.4×10^{-5} S cm^{-1} were obtained for LLTaO. Although Wang et al. [10] already reported a reduced sintering temperature for the solid solution $Li_{7-x}La_3Zr_{2-x}Ta_xO_{12}$ in the range from $x = 0.2$ to $x = 2$ when $NaHCO_3$ and α-Al_2O_3 were used as sintering additives, the influence of Al on the sintering behavior of LLTaO has not been investigated in detail yet. In contrast, there were reports about the role of Al regarding sintering of LLZ. For LLZ, an interaction between Al_2O_3 crucibles and the garnet material during sintering was observed. While unsubstituted LLZ exhibits a tetragonal structure[20], minor amounts of Al originating from Al_2O_3 crucibles diffuse and stabilize the fast-ion-conducting cubic structure[21]. Further, deliberate addition of Al_2O_3 powder as a sintering aid led to increased relative densities of LLZ specimens and hence afforded increased ionic conductivities[22, 23]. Al-rich glassy phases were observed at the grain boundaries of the material. These phases may also contain Li, which cannot be detected by energy dispersive X-ray spectroscopy (EDS), which is usually employed for element detection when investigating the microstructure by scanning electron microscopy (SEM) [22–24]. In general, sintering of garnet-structured Li conductors is challenging, because Li-evaporation at elevated temperature leads to decomposition. This Li-loss occurs at temperatures above 1000 °C, whereas for sintering, higher temperatures between 1100 °C and 1200 °C are required. Thus, the decomposition takes place at lower temperatures than the densification of the material. Therefore, garnet sintering is usually carried out in powder beds made from the same material to compensate for the Li-evaporation. During sintering the Li evaporation from the powder leads to a higher Li partial pressure inside the closed crucible, and therefore the Li-evaporation from the pellet is suppressed. The impact of the powder bed composition on the resulting sample density and ionic conductivity also has not been investigated in the literature yet. Therefore, we carried out a detailed study on the effect of the composition of sintering beds on the relative density in unsubstituted as well as Al-containing LLTaO.

2. Materials and methods

$Li_5La_3Ta_2O_{12}$ (LLTaO) and $Li_{4.4}Al_{0.2}La_3Ta_2O_{12}$ (Al-LLTaO) were synthesized by a solid-state reaction. LiOH • H_2O (VWR, 99%), La_2O_3 (Inframat, 99.99%, dried for 12h in air at 900 °C before use), Ta_2O_5 (Inframat, 99.99%) and Al_2O_3 (Inframat, 99.9%) were mixed in stoichiometric amounts with a Li-excess of 10 at.-% (LLTaO) or 20 at.-% (Al-LLTaO). The mixture was dry milled with a Retsch RM200 automatic mortar grinder, pressed into pellets and calcined in air at 700°C for 24 h in Al_2O_3 crucibles. After that, the pellets were dry milled and pressed again for a second air calcination step at 900 °C, which lasted 24 h. After these calcinations, X-ray diffraction (XRD) data showed that $Li_5La_3Ta_2O_{12}$ (ICSD#68252) was formed as a single phase in case of the unsubstituted LLTaO. In case of Al-LLTaO, $Li_5La_3Ta_2O_{12}$ was identified as the main phase, and small amounts of a secondary phase consisting of $LaAlO_3$ were observed (see supplementary information S1).

Sintering was carried out in alumina crucibles. A powder (i.e., sintering bed) was placed inside the crucibles. The pellets were put on the powder bed, and also completely covered with powder. The crucibles were covered with an alumina lid. LLTaO and calcined $Li_{6.54}Al_{0.02}La_3Zr_{1.6}Ta_{0.4}O_{12}$ (Al,Ta-LLZ; nominal composition) were used as the powder beds for sintering LLTaO. The synthesis of Al,Ta-LLZ was already described by Tsai et al. [24,25]. Al-LLTaO was sintered in Al-LLTaO and Al,Ta-LLZ powder beds, respectively. All samples were sintered for 24 h in air at 1200 °C. After sintering, the powders that were attached to the surface of the pellets were removed by polishing with SiC abrasive papers, and the relative densities were determined by the geometrical method.

XRD was carried out with a Bruker D4 endeavor using Cu-K$_\alpha$ radiation in Bragg-Brentano geometry.

Cross sections were prepared by embedding the specimens in epoxy resin, grinding and polishing with SiC abrasive paper. The final polishing step was done with a water-free polishing suspension. SEM images were obtained with a Zeiss Ultra 55 SEM (Carl Zeiss NTS GmbH, Germany) equipped with an INCAEnergy 400 EDS detector (Oxford Instruments) and a Hitachi TM3000 tabletop SEM equipped with a Bruker Quantax 70 EDS detector.

Inductively-coupled plasma optical emission spectroscopy (ICP-OES) was carried out to determine the chemical composition. The samples were dissolved in aqueous solution through different processes (details can be found in the supplementary information). The measurements were carried out with an iCAP 6500 instrument (ThermoScientific) for the calcined powders and an iCAP 7600 device (ThermoScientific) for the sintered materials.

The ionic conductivities of the samples were determined by electrochemical ac impedance spectroscopy (EIS) using a BioLogic VMP-300 multipotentiostat. Temperature dependent EIS measurements were carried out between -30 °C and 80 °C using a climate chamber (Vötsch VT4002). Before each measurement, the temperature was held for 3 h to ensure a homogenous temperature distribution in the sample. Au layers functioning as blocking electrodes were sputtered by dc sputtering on the polished top and bottom surfaces of sintered pellets. The data was recorded in the frequency range from 3 MHz to 100 mHz with a perturbation amplitude of 10 mV. ZView® (Scribner Associates) software was used for the analysis.

3. Results

To investigate the impact of Li and the Al content in the bulk structure and/or in the sintering atmosphere on the densification and ionic conductivity of LLTaO-based garnets, different combinations of green bodies (i.e., powder pellets pressed in ambient atmosphere) and powder beds have been considered. The investigated combinations are shown in Table 2. It should be noted that sintering without utilizing a powder bed resulted in no significant densification in the temperature range between 1000 °C and 1200 °C with a dwell time of 4 h in comparison to the pressed non-sintered samples. Longer sintering times, i.e., 24 h, led to a decomposition of the material without any densification (see supplementary information, S2).

Table 1
Literature overview of relative density and ionic conductivity of $Li_5La_3Ta_2O_{12}$ in dependence of sintering parameters.

Method	Was a powder bed used?	Sintering temperature /°C	Sintering time	Relative density /%	Total conductivity /S cm^{-1}	Temperature of total conductivity measurement /°C	E_a /eV	Ref.
Free sintering	Not mentioned	950	24h	–	3.4×10^{-6}	25	0.56	[9]
Free sintering (with sintering aid)	Yes, with similar composition	1230	36 h	93.8	3.4×10^{-5}	25	–	[10]
Free sintering	Not mentioned	850	24 h	71	5.4×10^{-7}	40	0.62	[11]
Free sintering	Yes, with similar composition	900	24 h	–	1.06×10^{-6}	33	0.6	[12]
Free sintering	Yes, with similar composition	1150	12 h	–	1.3×10^{-5}	25	0.491	[13]
Spark-plasma sintering	Not mentioned	1000	10 min	–	7.3×10^{-6}	27	–	[14]
Self consolidation	Not mentioned	1150	20 h	95	2.63×10^{-5}	30	0.54	[15]

Table 2
Relative densities of $Li_5La_3Ta_2O_{12}$ and $Li_{4.4}Al_{0.2}La_3Ta_2O_{12}$ sintered in diffe1rent powder beds (determined by geometrical method; nominal stoichiometry).

Pellet material / Powder bed	$Li_5La_3Ta_2O_{12}$ (LLTaO)	$Li_{4.4}Al_{0.2}La_3Ta_2O_{12}$ (Al-LLTaO)
$Li_5La_3Ta_2O_{12}$ (LLTaO)	**(A)** 58–62%	–
$Li_{4.4}Al_{0.2}La_3Ta_2O_{12}$ (Al-LLTaO)	–	**(C)** 78–82%
$Li_{6.54}Al_{0.02}La_3Zr_{1.6}Ta_{0.4}O_{12}$ (Al, Ta-LLZ)	**(B)** 79–85%	**(D)** 85–89%

All green bodies showed a relative density of about 60% after uniaxial pressing. The relative densities of the samples that were sintered in different powder beds at 1200°C for 24h are listed in Table 2. Hardly any densification was observed for sample A. Sometimes even a lower relative density was observed, which can be explained by a loss of mass, caused by Li-loss, evaporation of water and the decomposition of carbonates on the powder surface. When Al,Ta-LLZ was used as the sintering bed instead of LLTaO (sample B), the relative density of the sintered bodies increased to 79–85%. As already mentioned before, the addition of small amounts of Al improved the sintering behavior of LLZ garnets [22]. The synthesized Al-LLTaO that was sintered in an Al-LLTaO powder bed (sample C) also showed improved relative densities of 78–82%. The relative density was further increased to 90% when Al-LLTaO was sintered in an Al,Ta-LLZ powder bed (sample D). However, in batches (samples B and D) sintered with Al,Ta-LLZ up to 50% of the samples were damaged due to severe cracking. Since high stresses are necessary to cause cracks, inhomogenous sintering is the most likely explanation for the formation of cracks. In comparison, no cracks were observed when the composition of the pellets and the powder beds was identical. It can be assumed that cracking is enhanced by direct contact between the powder bed and the pellet. For future investigations, it is therefore advisable to choose a different experimental setup, e.g. the setup already chosen for sintering garnets with Li_2CO_3 powder bed by Huang et al. [26].

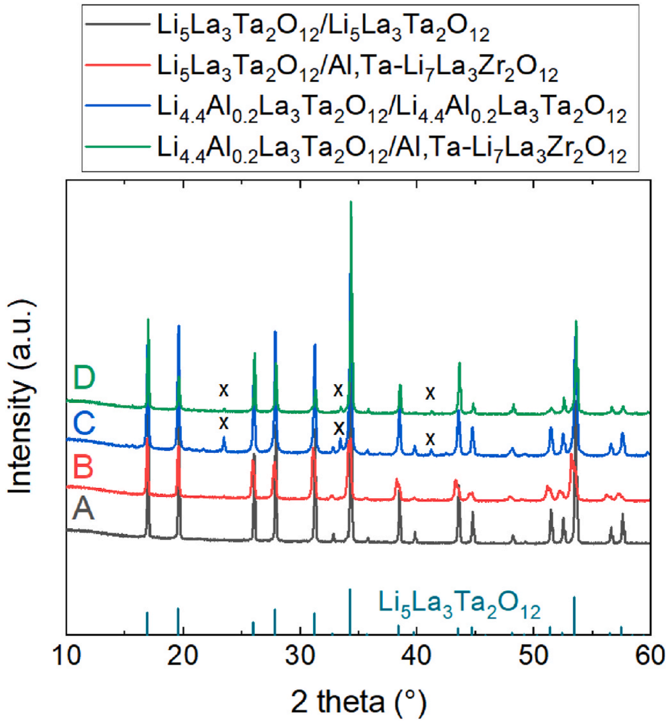

Fig. 1. X-ray diffraction patterns of $Li_5La_3Ta_2O_{12}$ and $Li_{4.4}Al_{0.2}La_3Ta_2O_{12}$ sintered in different powder beds. The $Li_5La_3Ta_2O_{12}$ pattern was generated from ICSD 68252, x indicates the $LaAlO_3$ secondary phase.

The X-ray diffraction patterns of the sintered samples shown in Fig. 1 reveal that the LLTaO samples exhibited a cubic garnet structure after sintering, irrespective of the type of powder bed used. The Al-LLTaO specimens consisted of garnet-type LLTaO as the main phase and the $LaAlO_3$ impurity, which still remained in the samples after sintering. The intensity of the peaks corresponding to $LaAlO_3$ was reduced when Al,Ta-LLZ was used as the powder bed, indicating a reduced amount of $LaAlO_3$ as secondary phase. The peak intensity of the $LaAlO_3$ secondary phase in sample C is increased in comparison to the initial powder. We assume that the crystallinity of $LaAlO_3$ increased during the sintering process. The calcination temperature was only 900°C, which may avoid complete crystallinity of the phases and therefore lead to a lower intensity of the phases peak's in the XRD pattern.

The microstructure of the samples as well as EDS mappings are shown in Fig. 2. Sample A evidently turned out to be highly porous. The EDS-mapping shows a uniform distribution of La and Ta throughout the material, while at the same time Al was not detected. The latter was also confirmed by the absence of the Al-K_α peak in the low energy regime of the EDS spectra (which correspond to the mappings in Fig. 2) shown in Fig. 3. Thus, a possible diffusion of Al from the Al_2O_3 crucible into the sample can be neglected.

Sample B shows a denser microstructure with larger grains than sample A. The sample contained only a few pores (darkest parts in the image). In this sample, La-rich precipitates were observed along with Al (two examples are marked by yellow circles), whereby Al-rich parts were also detected without La (two examples are marked by a blue circle). The local accumulation of Al was also confirmed by detailed point measurements (see Fig. 4). The irregular shape of the Al,La-rich phase (spectrum 1) suggests that this phase is glassy. From these measurements it can be concluded that Al–O rich as well as Al–La–O rich phases were formed after sintering. Since Li cannot be detected by the applied types of EDS detectors, both phases may also contain additional Li. The used LLTaO powder did not contain Al before sintering. Therefore, either Al,Ta-LLZ or the Al_2O_3 crucible acted as the Al source. Al not was detected in the main phase (spectrum 2).

Sample C shows smaller grains and pores than sample B with a similar density of the sample. The EDS-mappings reveal that Al is always accompanied by La, which is in agreement with the $LaAlO_3$ secondary phase obtained by XRD. Sample D stood out as an exaggerated grain growth was observed. Grains with sizes of several hundred microns are separated by thick grain boundaries and large cracks. Exaggerated grain growth has been observed for Al-containing LLZ also in prior work [27]. Inside the grains, pores and small precipitates are visible. This can be attributed to a rapid growth in which no pinning effect of the grain boundaries or secondary phases take place, so that the pores and secondary phases are trapped within the grain. The detailed EDS point measurements in Fig. 5 show only Ta and La signals for the main phase, and Al was not detected (spectrum 1 in Fig. 5). This means that Al is not integrated into the garnet structure of LLTaO (or integrated only in small amounts below the detection limit of EDS). Similar to the samples sintered in an Al-LLTaO powder bed (sample B), Al–La–O containing grains were detected by EDS (spectrum 2 in Fig. 5). However, additional dark phases which are rich in Al and O but do not contain La, similar to the Al-free sample sintered in Al,Ta-LLZ, were also observed for this sintering setup (spectrum 3 in Fig. 5).

In Table 3 the compositions of the sintered pellets in comparison to the calcined powders are listed. All values were determined by ICP-OES. The amount of Li in the sintered pellets is reduced in comparison to the calcined powders, which can be attributed to the evaporation of Li during the sintering process. When Al,Ta-LLZ was used as sintering bed, the final amount of Li in the samples was larger compared to sintering in a powder bed with a composition that was identical to the pellet. Minor amounts of Zr were also detected, which could not be verified by EDS measurements. Fig. 3 shows that the Zr-L_α peak was absent for all samples in the average EDS spectrum. However, SEM shows a more localized representation of the sample compared to what was analyzed

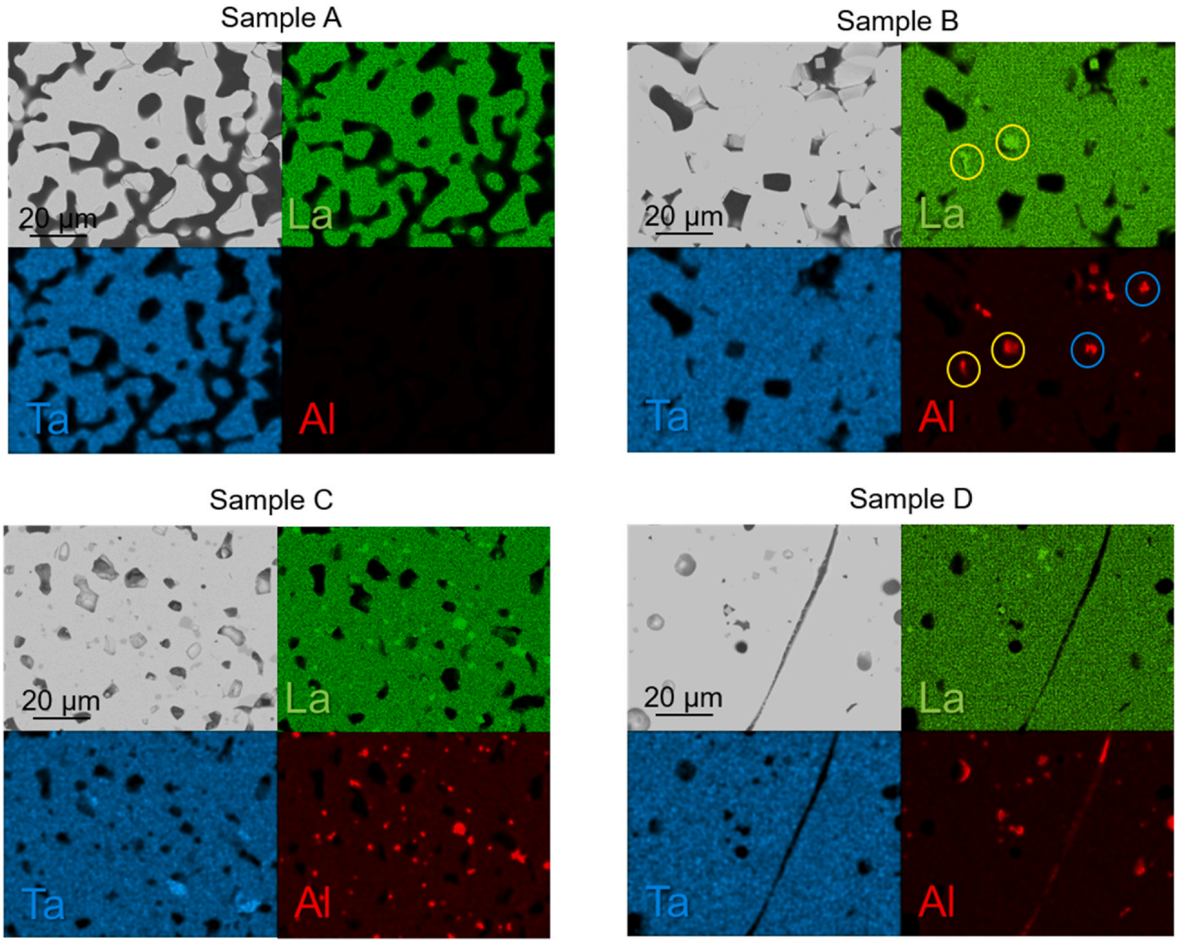

Fig. 2. SEM images and EDS-mapping of $Li_5La_3Ta_2O_{12}$ and $Li_{4.4}Al_{0.2}La_3Ta_2O_{12}$ sintered in different powder beds. Please note, that for Al-LLTaO sintered in Al,Ta-LLZ a region without large cracks was chosen. For this reason, the relative density appears higher in the SEM image than in the geometric measurement. The bright color shows the ceramic material, and the dark part represents the pores that are filled with epoxy resin. (For interpretation of the references to color in this figure legend, the reader is referred to the Web version of this article.)

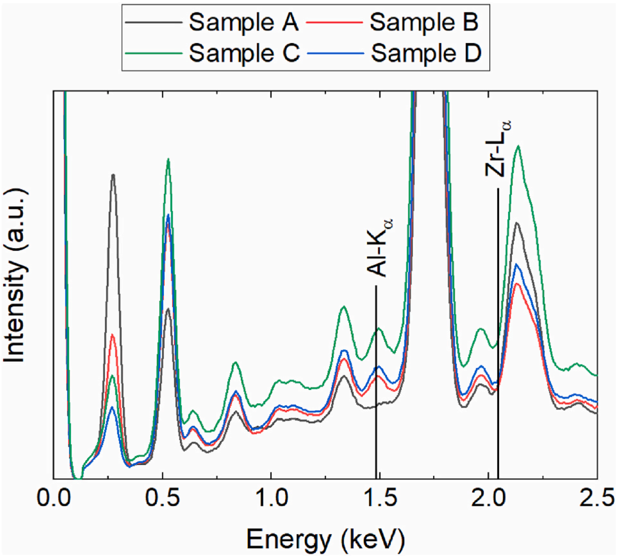

Fig. 3. Low-energy regime of the average EDS-spectra for the mappings shown in Fig. 2.

by ICP-OES. It is possible, that either residual powder from the sintering bed remained in the sample or that interdiffusion of Zr from the sintering bed into the sample occurred to a minor extent.

The variation of the Al content is the most interesting aspect when comparing the different samples. A small amount of Al, which is close to the detection limit of the measurement, was observed in the Al-free sample A. For sample B an increase in Al was detected, which was also confirmed by EDS. Sample C showed only a minor change of the Al-content in comparison to the calcined powder, which is in the range of the measurement error. For sample D, a significant loss of Al was detected, and the resulting amount of Al that remained was similar to that in sample B. Based on these results, and taking also into account the XRD and SEM results, we conclude that sample D loses Al during sintering.

The ionic conductivity was determined for samples with a density higher than 79%, because otherwise the surface could not be polished to have a sufficient quality for contact layer deposition. The impedance spectra that were determined using gold-electrodes are shown in Fig. 6a.

A semicircle at high frequencies was observed for all samples, most likely describing the ionic conductivity of the sample, and a tail/broad semicircle, most likely describing the blocking effect of the gold electrodes. The total conductivity was determined over the whole temperature range by using one or two R-CPE-elements to determine the total conductivity and two R-CPE elements to model the blocking tails.

The assignment of the elements to either the total conductivity or the gold-electrode/LLZ interface was done based the respective capacitance.

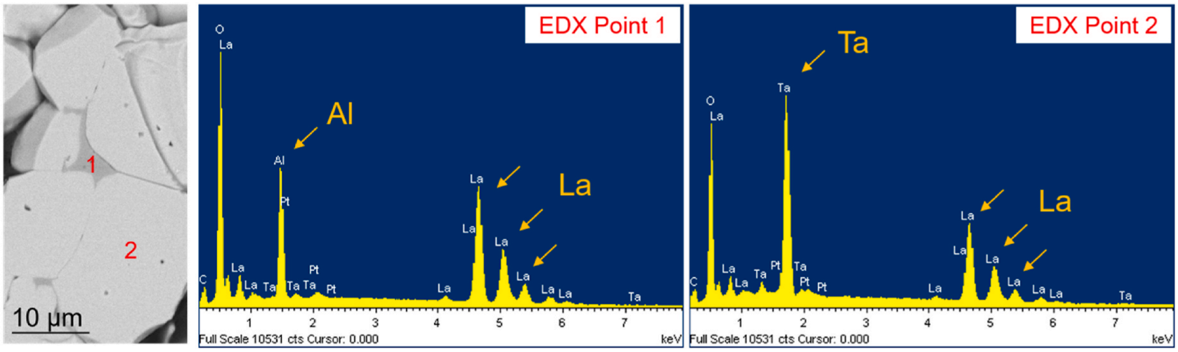

Fig. 4. Detailed BSE image of the microstructure and EDS point spectra of selected features in Sample B.

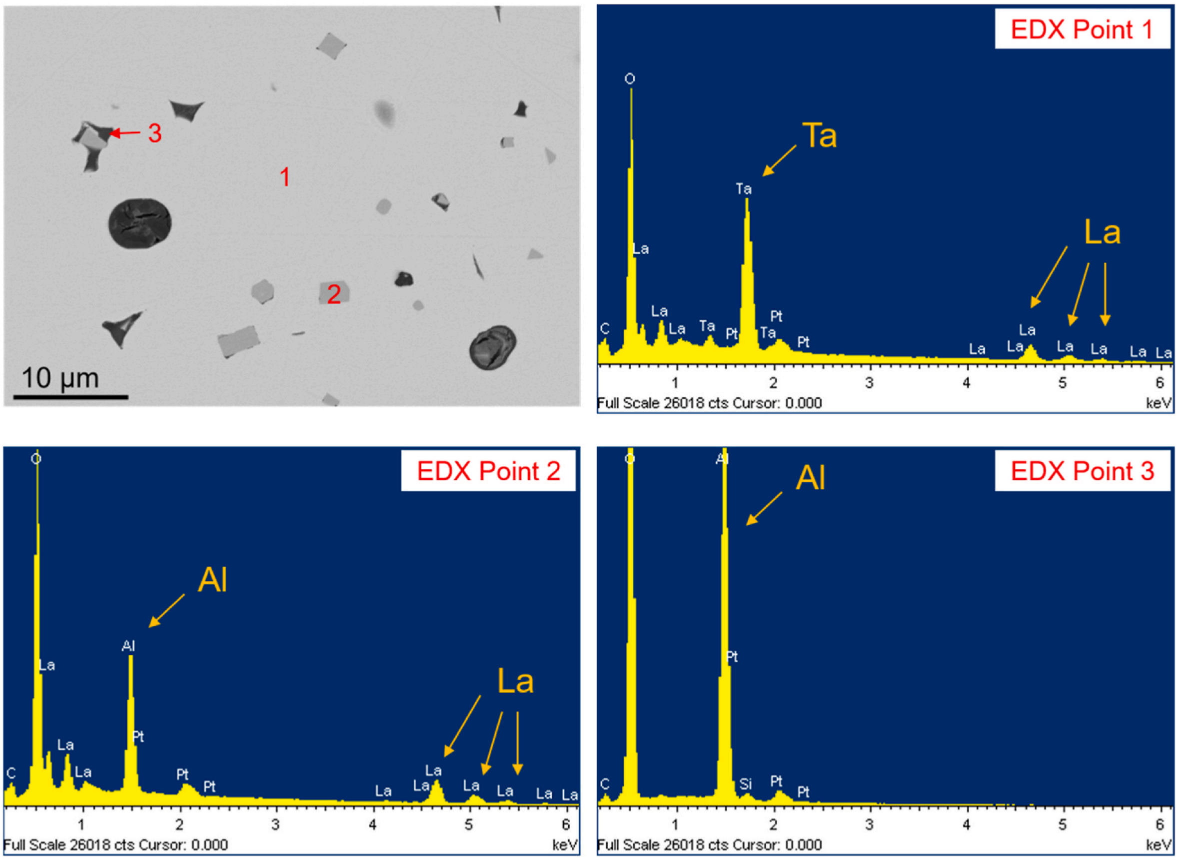

Fig. 5. Detailed BSE image of the microstructure and EDS point spectra of selected features in Sample D.

Table 3
Chemical composition of sintered bodies in comparison to calcined powders determined by ICP-OES measurements. All values were normalized to La = 3. Error values were calculated from the standard deviation of several measurements and do not include systematic measurement errors. If no error value is given, the error is smaller than 0.005. If no value is given, the element was not analyzed.

Sample	A	B	C	D	LLTaO calcined powder	Al,Ta-LLZ calcined powder	Al-LLTaO calcined powder
Li	4.97 ± 0.15	5.29 ± 0.32	4.87 ± 0.14	5.28 ± 0.29	5.56 ± 0.02	7.14 ± 0.04	5.43 ± 0.03
Al	0.02	0.05	0.16 ± 0.03	0.05	–	0.15	0.18 ± 0.01
La	3 ± 0.04	3 ± 0.08	3 ± 0.01	3 ± 0.01	3 ± 0.02	3 ± 0.01	3 ± 0.03
Zr	0.00	0.01	0.00	0.09	–	1.53 ± 0.01	–
Ta	1.95 ± 0.05	1.93 ± 0.13	1.88 ± 0.05	1.93 ± 0.02	1.93 ± 0.01	0.41	1.97 ± 0.01

The capacitances of the R-CPE elements contributing to the total conductivity were in the range of 10^{-9} F to 10^{-11} F, whereas the R-CPE elements of the electrode interface showed capacitances in the range of 10^{-6} F. The data did not show a clear separation between bulk and grain boundary conductivity, and therefore total conductivities were calculated.

The temperature dependent ionic conductivities in the range from -30 °C to 80 °C are shown in Fig. 6b. The activation energies were

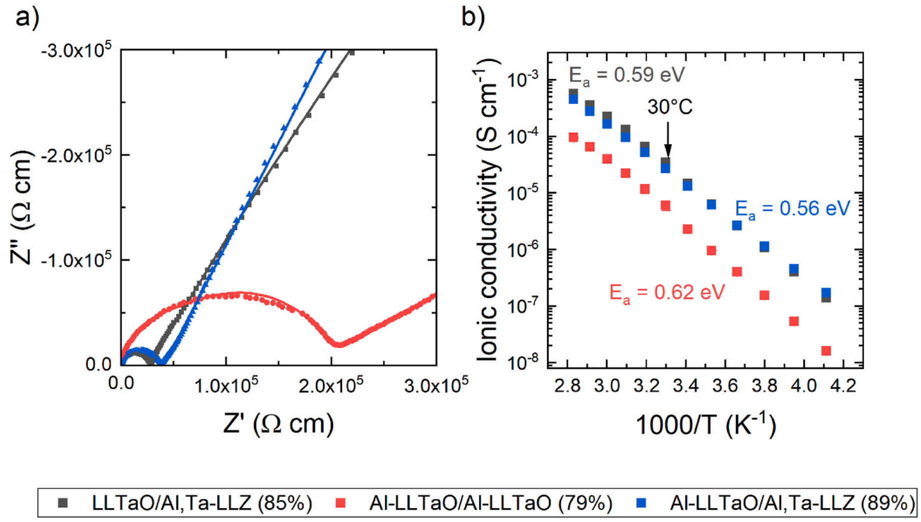

Fig. 6. a) Impedance spectra at 30° of $Li_5La_3Ta_2O_{12}$ and $Li_{4.4}Al_{0.2}La_3Ta_2O_{12}$ sintered in different powder beds b) Temperature dependent ionic conductivities of $Li_5La_3Ta_2O_{12}$ and $Li_{4.4}Al_{0.2}La_3Ta_2O_{12}$ sintered in different powder beds.

determined by employing the following equation:

$$\sigma T = A\ \exp\left(\frac{-E_a}{k_B T}\right)$$

Where σ is the ionic conductivity, A is the pre-exponential factor, E_a represents the activation energy, k_B represents the Boltzmann factor and T is the temperature. In Table 4 the determined conductivities and activation energies are compared to the relative densities of the samples and the chemical changes during the sintering process. These ionic conductivities are of similar magnitude as the literature data that is shown in Table 1.

As demonstrated above, the use of powder beds for sintering of garnets is a very efficient way to suppress the structure decomposition caused by the Li loss at high temperatures. However, when garnets with a low Li-content, such as LLTaO are used, the Li partial pressure generated from the powder bed can be insufficient, as was demonstrated for sample A. The sintering process could be improved by using an Al,Ta-LLZ powder bed. In this case, not only a higher Li-partial pressure was realized, but also Al was detected as an Al-rich phase at the grain boundary inside LLTaO after sintering.

In order to clarify the role of Al during sintering, Al-LLTaO was synthesized, and the sintering behavior was investigated. Sintering of Al-LLTaO in an Al-LLTaO powder bed led to improved sintering compared to LLTaO in LLTaO. However, the obtained relative density was rather low at about 80%. Higher relative densities of up to 90% were achieved by sintering in Al,Ta-LLZ. Based on these results one can conclude that both the Al- and Li-content in the sintering atmosphere have a significant influence on the sintering behavior of Li-containing garnets. In several publications, in which LLZ was investigated, the formation of liquid Li–Al–O phases at the grain boundaries during sintering was discussed. Such phases can facilitate densification through a liquid phase sintering process [23,24]. Possible candidates that can be formed during the heat treatment are Li_5AlO_4 or an eutectic mixture of $LiAl_5O_4$ with $LiAlO_2$, both with a melting point of about 1050 °C [28]. However, our experimental findings demonstrate that Al is lost from the sample after sintering. There are two mechanisms conceivable to explain the Al-loss from sample D. The first possibility is the absorption of Al from the powder bed. Since Al-LLTaO contains more Al than Al, Ta-LLZO, Li–Al–O-phases can be equally distributed over the whole powder-pellet-composite leading to a reduced amount of Al in the Al-LLTaO pellet. However, the Al-content of Al-LLTaO and Al,Ta-LLZO are quite similar, so that we will discuss a second possibility, although the first possibility is supported by the already known formation of liquid Li–Al–O phases during sintering of garnets. The second possibility would be the evaporation of Li–Al–O phases. The corroboration of this hypothesis requires a more detailed investigation of the phases formed during sintering while it is known that only Li and O rich species are reported to evaporate in Li_5AlO_4 and $LiAlO_2$ [29]. Furthermore, excess Al is bound in $LaAlO_3$ in the initial Al-LLTaO powder. It is therefore possible that La also plays a role in the Al-loss mechanism. However, the required thermodynamic data about phase stabilities in the Al–Li–La–O system is not available from the literature. Thus, the possible mechanism for Al-loss still remains unclear.

Table 4
Relative density, changes in chemical composition as well as ionic conductivity and activation energy for the investigated samples; p.f.u. = per formula unit.

Sample	A	B	C	D
Relative density /%	60	85	79	89
Change of Li /p.f.u.	−0.59	−0.27	−0.56	−0.15
Change of Al /p.f.u.	+0.02	+0.05	−0.02	−0.13
Ionic conductivity /S cm^{-1}	–	3.4×10^{-5}	6.0×10^{-6}	2.6×10^{-5}
Activation energy /eV	–	0.59	0.62	0.56

The absence of Al-peaks in the EDS spectra suggests that a much lower amount of Al can be incorporated into the LLTaO crystal lattice compared to the LLZ crystal lattice, where up to 0.2 mol Al per formula unit (p.f.u.) were reported. In sample B, the Al-content was determined to be 0.05 p.f.u., whereby Al-containing secondary phases were clearly detectable by SEM. For this reason, it can be assumed that the maximum amount of Al that can be incorporated into the LLTaO crystal structure is below 0.05 p.f.u. Thus, in our experimental set-up a much higher amount of Al was available for the formation of species that enhance grain growth and act as sintering aids relative to the comparable LLZ sintering processes.

The obtained ionic conductivities of the samples show the lowest value for sample C, which has the lowest relative density as well as the lowest Li-content. The other two samples have only small differences in ionic conductivity, relative density and Li-content. The Al- and Li-contents of both samples are similar, and it was also shown that the main phase does not uptake significant amounts of Al, so that it can be assumed that the Li and Al distribution between the grains and grain boundaries of both samples is similar. From this point of view it is somewhat surprising that the lower relative density shows a slightly higher conductivity. However, a closer look at the microstructure shows that in case of sample D the large grains are sometimes isolated, so that a sufficient percolation of Li-ions is not always possible. In contrast, the microstructure of the sample B specimen shows a better connection of the particles and thinner grain boundaries. These differences in the microstructure can explain the small difference in the ionic conductivity. This assumption is confirmed by the detailed result of impedance spectroscopy, which is shown in supplementary information. The ratio of bulk resistance to grain boundary resistance (R_b / R_{gb}) for sample D is about 3 whereas the ratio for sample B is 13.9, showing a smaller contribution of the grain boundaries to the total resistance in sample B.

It should be emphasized that the optimization of the powder bed composition based on the deeper understanding of sintering parameters helps to improve the density and ionic conductivity of garnets significantly without the use of sintering additives, which can potentially change the grain boundary composition and the related mechanical and electrochemical properties. Thus, the ionic conductivity obtained for the sintered ceramics in this work are similar to the highest LLTaO conductivity values published by Wang et al. [10], who, however, achieved similar relative densities by applying sintering additives.

4. Conclusions

The presence of Al and Li has a strong influence on the sintering behavior of LLTaO ceramics. Without additional aluminum, densification through sintering was not observed, even at temperatures as high as 1200 °C. By addition of Al to the sintering body (Al-LLTaO), the sintering behavior was improved significantly. Further densification can be achieved by employing a Li-rich powder bed. In this work, we utilized calcined Al,Ta-LLZ. Under these conditions, both materials, LLTaO and Al-LLTaO, were sintered while achieving high relative densities between 85% and 90%. These results show that while the presence of Al promotes sintering, an excess of Li must also be present to achieve relative densities around 90%. The lower amount of Li-excess in Li-reduced garnets, such as LLTaO, may well be the cause of the fairly low relative densities and low ionic conductivities that were reported in the past.

The results from this work are relevant not only for deriving processing strategies for garnets. Any process, for which sintering beds are applied to compensate for the loss of volatile species, can potentially be improved by probing the influence of the composition of the sintering bed on densification and phase formation in the context of functional ceramic materials.

Declaration of competing interest

The authors declare that they have no known competing financial interests or personal relationships that could have appeared to influence the work reported in this paper.

Acknowledgement

The financial support by the Bundesministerium für Bildung und Forschung (Federal ministry of education and research), Germany, under projects no. 13N9973, 03X4634C, 03SF0477A, and 13XP0173A is gratefully acknowledged. We thank Olivier Guillon for the discussion of the manuscript and Volker Bader for the technical support.

Appendix A. Supplementary data

Supplementary data to this article can be found online at https://doi.org/10.1016/j.oceram.2022.100268.

References

[1] R. Murugan, V. Thangadurai, W. Weppner, Fast lithium ion conduction in garnet-type Li7La3Zr2O12, Angew. Chem. Int. Ed. 46 (41) (2007) 7778–7781.

[2] L. Buannic, B. Orayech, J.-M. López Del Amo, J. Carrasco, N.A. Katcho, F. Aguesse, et al., Dual substitution strategy to enhance Li+ ionic conductivity in Li7La3Zr2O12 solid electrolyte, Chem. Mater. 29 (4) (2017) 1769–1778.

[3] C. Wang, K. Fu, S.P. Kammampata, D.W. McOwen, A.J. Samson, L. Zhang, et al., Garnet-type solid-state electrolytes: materials, interfaces, and batteries, Chem. Rev. 120 (10) (2020) 4257–4300.

[4] C.-L. Tsai, S. Yu, H. Tempel, H. Kungl, R.-A. Eichel, All-ceramic Li batteries based on garnet structured Li7La3Zr2O12, Mater. Technol. 35 (9–10) (2020) 656–674.

[5] R. Chen, Q. Li, X. Yu, L. Chen, H. Li, Approaching practically accessible solid-state batteries: stability issues related to solid electrolytes and interfaces, Chem. Rev. 120 (14) (2020) 6820–6877.

[6] L. Miara, A. Windmüller, C.-L. Tsai, W.D. Richards, Q. Ma, S. Uhlenbruck, et al., About the compatibility between high voltage spinel cathode materials and solid oxide electrolytes as a function of temperature, ACS Appl. Mater. Interfaces 8 (40) (2016) 26842–26850.

[7] S. Uhlenbruck, J. Dornseiffer, S. Lobe, C. Dellen, C.-L. Tsai, B. Gotzen, et al., Cathode-electrolyte material interactions during manufacturing of inorganic solid-state lithium batteries, J. Electroceram. 38 (2016) 197–206, https://doi.org/10.1007/s10832-016-0062-x.

[8] Y. Ren, T. Liu, Y. Shen, Y. Lin, C.-W. Nan, Chemical compatibility between garnet-like solid state electrolyte Li6.75La3Zr1.75Ta0.25O12 and major commercial lithium battery cathode materials, J Materiomics 2 (3) (2016) 256–264.

[9] V. Thangadurai, H. Kaack, W.J.F. Weppner, Novel fast lithium ion conduction in garnet-type Li5La3M2O12 (M = Nb, Ta), J. Am. Ceram. Soc. 86 (3) (2003) 437–440.

[10] Y. Wang, W. Lai, High ionic conductivity lithium garnet oxides of Li7−xLa3Zr2−xTaxO12 compositions, Electrochem. Solid State Lett. 15 (5) (2012) A68–A71.

[11] C.R. Mariappan, K.I. Gnanasekar, V. Jayaraman, T. Gnanasekaran, Lithium ion conduction in Li5La3Ta2O12 and Li7La3Ta2O13 garnet-type materials, J. Electroceram. 30 (4) (2013) 258–265.

[12] S. Ramakumar, N. Janani, R. Murugan, Influence of lithium concentration on the structure and Li+ transport properties of cubic phase lithium garnets, Dalton Trans. 44 (2) (2015) 539–552.

[13] H. Nemori, Y. Matsuda, S. Mitsuoka, M. Matsui, O. Yamamoto, Y. Takeda, et al., Stability of garnet-type solid electrolyte LixLa3A2-yByO12 (A=Nb or Ta, B=Sc or Zr), Solid State Ionics 282 (2015) 7–12.

[14] M. Kotobuki, S. Song, R. Takahashi, S. Yanagiya, L. Lu, Improvement of Li ion conductivity of Li5La3Ta2O12 solid electrolyte by substitution of Ge for Ta, J. Power Sources 349 (2017) 105–110.

[15] P. Zhao, Y. Xiang, Y. Xu, Y. Wen, W. Zhang, X. Zhu, et al., Enhancement of density and ionic conductivity for garnet-type Li5La3Ta2O12 solid electrolyte by self-consolidation strategy, Ceram. Int. 44 (8) (2018) 9105–9111, https://doi.org/10.1016/j.ceramint.2018.02.118.

[16] S. Lobe, C. Dellen, A. Windmüller, C.L. Tsai, F. Vondahlen, S. Uhlenbruck, et al., Challenges regarding thin film deposition of garnet electrolytes for all-solid-state lithium batteries with high energy density, Ionics 24 (2018) 2199–2208, https://doi.org/10.1007/s11581-018-2594-3.

[17] S. Lobe, C. Dellen, M. Finsterbusch, H.G. Gehrke, D. Sebold, C.L. Tsai, et al., Radio frequency magnetron sputtering of Li7La3Zr2O12 thin films for solid-state batteries, J. Power Sources 307 (2016) 684–689.

[18] R. Pfenninger, M. Struzik, I. Garbayo, E. Stilp, J.L.M. Rupp, A low ride on processing temperature for fast lithium conduction in garnet solid-state battery films, Nat. Energy 4 (6) (2019) 475–483.

[19] S. Lobe, A. Bauer, S. Uhlenbruck, D. Fattakhova-Rohlfing, Physical vapor deposition in solid-state battery development: from materials to devices, Adv. Sci. (2021), 2002044 n/a(n/a).

[20] J. Awaka, N. Kijima, H. Hayakawa, J. Akimoto, Synthesis and structure analysis of tetragonal Li7La3Zr2O12 with the garnet-related type structure, J. Solid State Chem. 182 (8) (2009) 2046–2052.

[21] C.A. Geiger, E. Alekseev, B. Lazic, M. Fisch, T. Armbruster, R. Langner, et al., Crystal chemistry and stability of "Li7La3Zr2O12" garnet: a fast lithium-ion conductor, Inorg. Chem. 50 (3) (2011) 1089–1097.

[22] N.C. Rosero-Navarro, A. Miura, M. Higuchi, K. Tadanaga, Optimization of Al2O3 and Li3BO3 content as sintering additives of Li7−xLa2.95Ca0.05ZrTaO12 at low temperature, J. Electron. Mater. 46 (1) (2017) 497–501.

[23] Y. Wang, P. Yan, J. Xiao, X. Lu, J.-G. Zhang, V.L. Sprenkle, Effect of Al2O3 on the sintering of garnet-type Li6.5La3Zr1.5Ta0.5O12, Solid State Ionics 294 (2016) 108–115.

[24] C.-L. Tsai, V. Roddatis, C.V. Chandran, Q. Ma, S. Uhlenbruck, M. Bram, et al., Li7La3Zr2O12 interface modification for Li dendrite prevention, ACS Appl. Mater. Interfaces 8 (16) (2016) 10617–10626.

[25] C.-L. Tsai, Q. Ma, C. Dellen, S. Lobe, F. Vondahlen, A. Windmüller, et al., A garnet structure based all-solid-state Li battery without interface modification: resolving incompatibility issue on positive electrode, Sustain. Energy Fuels 3 (2019) 280–291, https://doi.org/10.1039/C8SE00436F.

[26] Z. Huang, K. Liu, L. Chen, Y. Lu, Y. Li, C.-A. Wang, Sintering behavior of garnet-type Li6.4La3Zr1.4Ta0.6O12 in Li2CO3 atmosphere and its electrochemical property, Int. J. Appl. Ceram. Technol. 14 (5) (2017) 921–927.

[27] C.-L. Tsai, E. Dashjav, E.-M. Hammer, M. Finsterbusch, F. Tietz, S. Uhlenbruck, et al., High conductivity of mixed phase Al-substituted Li7La3Zr2O12, J. Electroceram. (2015) 1–8.

[28] H.J. Byker, I. Eliezer, N. Eliezer, R.A. Howald, Calculation of a phase diagram for the lithium oxide-aluminum oxide (LiO0.5-AlO1.5) system, J. Phys. Chem. 83 (18) (1979) 2349–2355.

[29] Y. Ikeda, H. Ito, G. Matsumoto, H. Hayashi, The vaporization and thermochemical stability of lithium aluminates, J. Nucl. Mater. 97 (1) (1981) 47–58.